

# 8 Pose Estimation of Multi-Part Curved Objects

Mourad Zerroug and Ramakant Nevatia

## 8.1 Introduction

Recognizing 3-D objects from a 2-D image is important for many visual tasks. Part of this problem is the estimation of the 3-D pose of the viewed objects. Alignment, introduced by [134], is a very attractive method since it is simple and efficient. Most objects demonstrated under the alignment technique are those for which low-level image features can be identified and matched with model features. These include polyhedra and objects with sharp corners or distinguished lines. Dealing with complex, curved, objects is more difficult because no such low-level features may be identifiable. This is due to the possible view-dependency of the outlines which may vary wildly with changes in viewpoint and thus are hard to match with object models.

Few efforts have addressed the pose estimation of curved objects. Kriegman and Ponce [136] use a complex method based on elimination theory which finds the pose by minimizing an objective function which is the distance between the viewed silhouettes and the projection of an algebraic surface representation of object models. The method of [131] addresses surfaces of revolution, a somewhat restricted class. A recent method of [139] uses invariants based on the cross-ratio along surfaces of revolution having bi-tangents. The above methods have been demonstrated on relatively simple, though curved, objects.

In this paper, we show that alignment-like techniques can still be used for a large class of complex, curved, multi-part objects provided adequate features and representations are used. More specifically, we demonstrate that high-level descriptions, based on a part-based formalism using generalized cylinders, provide means to establish *quasi-invariant* correspondences (meaning that they are almost exact over almost all viewpoints) between image and model shapes. These correspondences are in terms of powerful intrinsic quantitative shape attributes such as the axis, the scaling function and the cross-section of a part. The idea is that although the outlines may be viewpoint dependent, or may not have distinguished points, the derived shape descriptions in terms of the above powerful attributes (and their combinations) provide viewpoint independent entities which can be put into correspondence with models so represented. We believe this to be an important demonstration of the usefulness of high-level, part-based, descriptions in extending the classes of shapes which can be handled. The classes of shapes demonstrated here currently include arrangements of SHGCs (*straight homogeneous generalized cylinders*), a straight-axis primitive, and

PRGCs (*planar right generalized cylinders*), a curved (planar) axis primitive, a fairly large class of man-made objects (an image of such shapes is shown in Figure 8.1).

Although high-level descriptions have been used in the past in object recognition, they have been used largely for qualitative image-model matching [129,132,140]; we believe their use for quantitative pose estimation to be novel in this work. The method described here is inspired by the results of [146] which demonstrated that GC part-based descriptions can be obtained even in the presence of adverse imaging effects such as clutter and occlusion. Our approach is to use these descriptions to recognize the viewed objects and estimate their 3-D pose.

For lack of space, we will not describe the matching techniques in great detail. Rather, we emphasize the discussion on the use of the high-level part-based descriptions to establish image-model correspondences for relatively complex, curved, structured objects and demonstrate the application of alignment-like methods on those descriptions. However, we would like to emphasize that our method does not assume that model objects with which the viewed objects should be matched are selected by some previous process. Rather, it automatically finds the matching objects from the database and computes their pose.

In this paper, we discuss the computation of the scaled orthographic pose (which is reasonable for each object relatively far from the camera). The results can be used as initial estimates for the computation of the perspective pose as discussed in [134].

We organize the paper as follows. In section 8.2, we describe the representations used and the classes of objects addressed in this paper. In section 8.3, we discuss the use of these descriptions to solve the pose estimation of structured objects, and demonstrate the method on several real images of relatively complex objects. We conclude in section 8.4.

## 8.2 Representations

In this section, we describe the descriptions used to represent image and model objects.

### 8.2.1 Image Objects

Image objects are extracted using the method of [146]. This latter produces a graph representation of each viewed object without any prior knowledge of its identity. Rather, it uses purely generic tools to segment objects from the background and decompose their shapes into constituent generalized cylinder parts. A detailed description of the method is given by the authors of [145,146].

An important aspect of the results of that method is that it produces *projective shape descriptions* in that, although 2-D, the image characterizations of parts (such as their image axes and sweeps) correspond to the projection of the 3-D descriptions. This is very useful and, as we will show in section 8.3, allows the establishment of im-

age-model correspondences for objects for which alignment-like techniques haven't been demonstrated yet.

An example of descriptions is shown in Figure 8.1. Each detected object is described as a graph where nodes are parts and arcs labeled joint relationships between parts. For each part, the description consists of the following:

- a label giving its type (SHGC or PRGC)
- a label giving the type of sweep. For an SHGC, this label could be *cylinder*, *cone* or *non-linear* (the former two indicate a linear sweep while the latter indicates a non-linear one). For a PRGC, it could be *constant* or *non-constant*.
- the image of the cross-sections if visible. For an SHGC, the “top” cross-section is assumed visible.
- the image of the axis. In the case of SHGCs, for a *cylinder*, this consists of the *direction* of the axis, for a *cone* it consists of the *apex* and for a *non-linear* SHGC of a *line*. For a PRGC, this consists of a list of points which are in practice an excellent approximation of the projection of the 3-D axis [144].
- the pair-wise correspondences between the side boundaries which correspond to the projections of *co-cross-sectional* points in 3-D.
- for SHGCs, the description additionally includes a list of scaling ratios  $\{R_i; i = 1..n\}$  giving the amount of scaling of the cross-section at each position along the axis with respect to the top cross-section. The  $R_i$  values are *invariant under scaled orthographic projection* (quasi-invariant under perspective)..

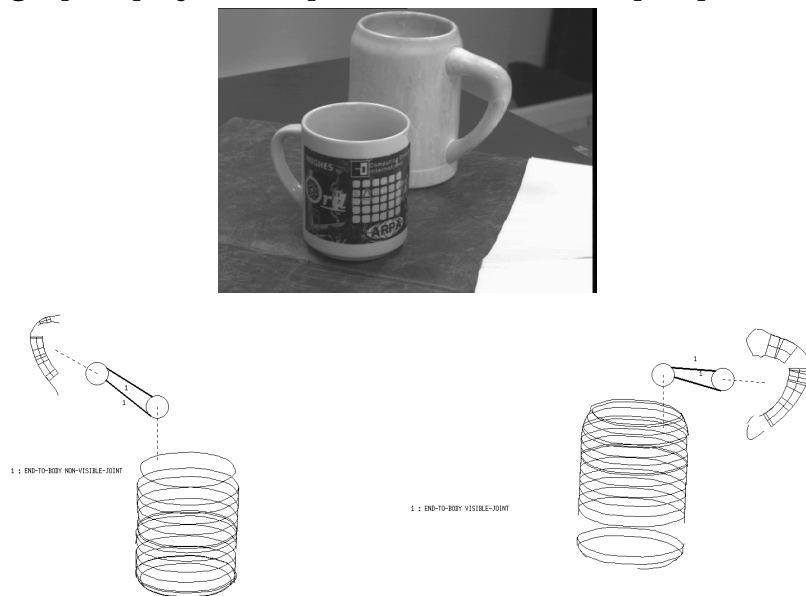


Figure 8.1 Descriptions (2-D) extracted from an image.

### 8.2.2 Model Objects

Each model object  $O_M$  is represented as a graph  $G_M = (Q_M, J_M)$  where  $Q_M = \{q_M^1, \dots, q_M^k\}$  is the set of its GC parts and  $J_M$  the set of labeled joints between the parts. Each part is represented by its 3-D intrinsic GC attributes; i.e. the cross-section, the axis and the scaling function all in a 3-D object-centered coordinate system  $S_q = (O_q, \vec{i}, \vec{j}, \vec{k})$ . Figure 8.2 illustrates this system for SHGCs and PRGCs. More specifically, the attribute representation consists of the following elements:

- the cross-section  $X_M$  represented as a list of points;  $X_M = \{p_i\}$
- the axis  $A_M$  which
  - for an SHGC is represented by the origin  $O_q$  (point of intersection of the straight axis with the cross-section plane) and its orientation  $\vec{N}_M$
  - for a PRGC is represented by the equation of its plane  $\Pi_M$  and quadratic B-splines giving an analytic expression of the axis points  $P_a^i$  and their tangent vectors  $\vec{T}_a$
- the scaling function  $R_M(z)$  giving for each arclength value  $z$  along the axis  $A_M$  the ratio  $R_M$  of the size of the cross-section at  $z$  with respect to the size of a reference (e.g. “top”) cross-section

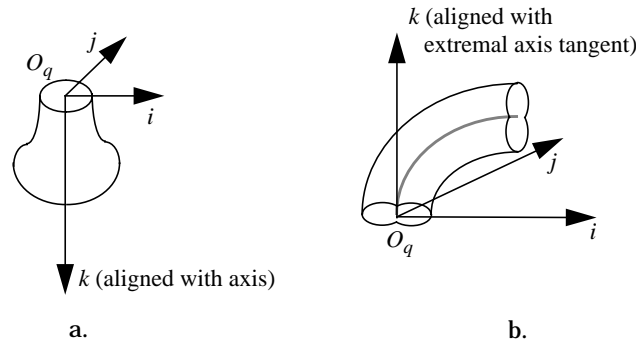


Figure 8.2 Object-centered part coordinate system for an SHGC (a); for a PRGC (b).

Figure 8.3 shows these representations for one of the object models used in the current experimentation.

### 8.3 Pose Estimation

Given extracted image descriptions, a matching stage is first applied in order to automatically determine which of the model objects  $O_M$  corresponds to each image object  $O_I$ . This process uses qualitative attributes of both image and model objects (such as part label, sweep type, joint label) in a graph matching method. For lack of space, we will not describe the matching step in this paper. It results in pairings between image and model objects and for each of them, the pairings between image and model

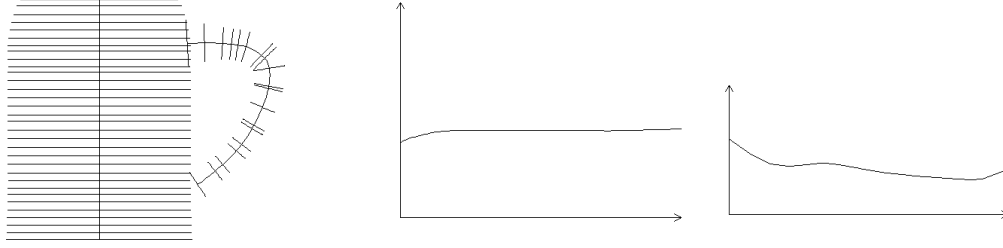


Figure 8.3 Representation of one of the model objects used in the experiments. Left: side view of the object also showing axes. Right: scaling functions of the object's parts (SHGC function is shown first).

parts. Each match ( $O_I, O_M$ ) can be used to estimate the pose of the viewed object. The method uses the GC-based descriptions to establish correspondences between the image and model parts. We first describe the coordinate systems used and identify the pose parameters.

### 8.3.1 Coordinate Systems and Pose Parameters

The world coordinate system  $W_S = (O, \vec{x}, \vec{y}, \vec{z})$  is chosen so that the  $x$ - and  $y$ -directions coincide with those of the image plane whose coordinate system is  $I_S = (O, \vec{x}, \vec{y})$ . For each object, a reference part  $q_{\text{ref}}$  is chosen. Each part's representation also includes the transformation  $T_i$  between its own coordinate system  $S_q = (O_q, i, j, k)$  and the one of  $q_{\text{ref}}$ . Currently, we assume that one of the parts is an SHGC which is chosen to be  $q_{\text{ref}}$  (which of the SHGCs, if many, is not important).

A model object  $O_M$  is represented in  $W_S$  such that the coordinate system of  $q_{\text{ref}}$  coincides with  $W_S$ . See Figure 8.4.a. Thus, through the transformations  $T_i$  and the relationship between the coordinate systems of  $q_{\text{ref}}$  with  $W_S$ , we can determine the pose of each part with respect to  $W_S$ . To model the viewing geometry, we use scaled orthographic (weak perspective) projection; i.e. we assume that objects' dimensions are small compared to their distance to the camera. In this model, the depth of a viewed object is taken to be the depth of a reference point  $P_0 = (x_0, y_0, z_0)^t_{W_S}$  on that object. In this case, the projection of a vector  $V = P - P_0$  is equivalent to an orthographic projection (along the  $z$ -direction) followed by a homogeneous scaling  $k$  in the image. Note that scaled orthography is used locally for each object, not the entire scene. As such, each object will have a different scaling factor  $k$ . The pose of a viewed object is determined by finding the transformation  $\mathbf{T}(P) = \mathbf{R} P + \mathbf{t}$  such that the projection of  $\mathbf{T}(O_M)$  coincides with  $O_I$ ; i.e.

$$p = \mathbf{SO}(\mathbf{T}(P)) = \mathbf{SO}(\mathbf{R} P + \mathbf{t}) \quad (8.1)$$

where  $\mathbf{R}$  is a rotation matrix,  $\mathbf{t}$  a translation vector,  $P$  is any point of  $O_M$  (all expressed in  $W_S$ ),  $p$  the projection (belonging to  $O_I$  and expressed in  $I_S$ ) of  $\mathbf{T}(P)$ , and  $\mathbf{SO}$  denotes scaled orthographic projection.

Because the third component of  $\mathbf{t}$  is not used, the pose under scaled orthographic projection is determined by 6 parameters, namely 3 for  $\mathbf{R}$  the first 2 components of  $\mathbf{t}$ , say  $t_x$  and  $t_y$ , and  $k$ . We model  $R$  as the product of three rotations

$$\mathbf{R} = \mathbf{R}_\phi \mathbf{R}_\sigma \mathbf{R}_\theta \quad (8.2)$$

where  $\mathbf{R}_\phi$  is a rotation about the  $z$ -axis by an angle  $\phi$ ,  $\mathbf{R}_\sigma$  a rotation about the  $x$ -axis by an angle  $\sigma$  and  $\mathbf{R}_\theta$  a rotation about the  $z$ -axis by an angle  $\theta$ . The whole sequence of transformations of equation (8.1) is illustrated in Figure 8.4.a-f.

Using the translated origin of the reference model part  $q_{\text{ref}}$  as the reference point  $P_0$ , the relationship between image and model coordinates is given by

$$u = k [\cos\theta (\cos\phi x - \sin\phi y) - \sin\theta \cos\sigma (\sin\phi x + \cos\phi y) + \sin\theta \sin\sigma z] + t_x \quad (8.3)$$

$$v = k [\sin\theta (\cos\phi x - \sin\phi y) + \cos\theta \cos\sigma (\sin\phi x + \cos\phi y) - \cos\theta \sin\sigma z] + t_y \quad (8.4)$$

where  $(u, v)$  denote image coordinates in  $I_S$  and  $(x, y, z)$  denote model coordinates in the system of  $q_{\text{ref}}$  (which, at its original pose, coincides with  $W_S$ ).

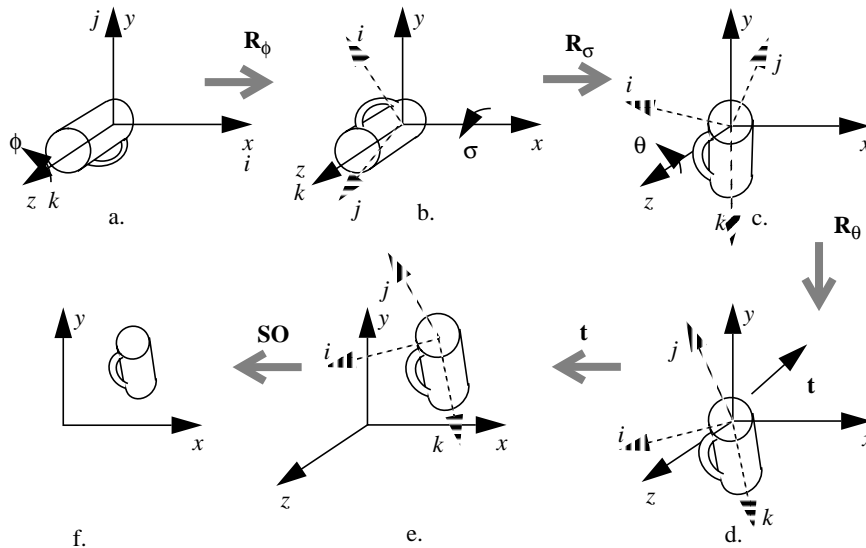


Figure 8.4 Sequence of transformations applied to the model object  $O_M$  so that its image coincides with  $O_I$ .

## 8.3.2 Establishing Correspondences for Single-Part Objects

### 8.3.2.1 SHGCs

#### 8.3.2.1.1 Non-linear SHGCs

In the case of a non-linear SHGC, for each cross-section  $X_{Ii}$  along the surface of the image SHGC ( $SHGC_I$ ), the scaling ratio  $R_{Ii}$  (available with the image description) it makes with the “top” cross-section is used to find the position  $z_i$  (which we will alternatively refer to as  $z$ -value, a missing element in the image description) on the model SHGC ( $SHGC_M$ ) it projects from. This is done by starting from the image “top” cross-section which is matched with the model “top cross-section” whose  $z$ -value is  $z_0=0$ <sup>1</sup>. Then, moving along the image axis, the  $z$ -value  $z_i$  corresponding to each image cross-section  $X_{Ii}$  along the surface of  $SHGC_I$  is chosen to be the one closest (and superior) to the previous  $z$ -value ( $z_{i-1}$ ) such that  $R_M(z_i) = R_{Ii}$ . This is done by “reading” the model scaling function in a table look-up fashion (see Figure 8.5). This process is not applied to cross-sections lying on constant regions of the scaling function since the correspondences would be ambiguous.

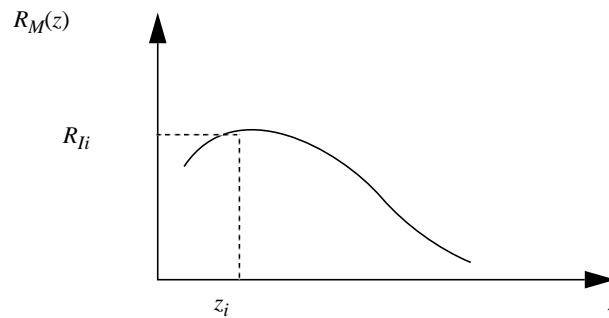


Figure 8.5 Finding correspondences between image cross-sections and model axis positions using the similarity of the invariant scaling ratios.

This results in a set of correspondences,

$$\{(X_{Ii}, z_i) \ i=0 \dots n\}$$

between image cross-sections and model positions (equivalently, model cross-sections  $X_M(z_i)$ ) on the SHGC axis. Many image-model point correspondences can now be established. From one of the invariant properties of SHGCs described in [145], the lines joining parallel symmetric points between any pair of cross-sections intersect at a single point (local apex) which belongs to the SHGC axis (Figure 8.6). Thus, the image local apex ( $A_{Ii}$ ) between each cross-section  $X_{Ii}$  ( $i > 0$ ) and  $X_{I0}$  corresponds to the model

---

1. the image “top” cross-section may also be matched with the model “bottom” cross-section in case the method fails. This amounts to considering the reverse parameterization of the model SHGC.

local apex ( $A_M(z_i)$ ) between each model cross-section  $X_M(z_i)$  ( $i > 0$ ) and  $X_M(0)$ . The local apices are determined analytically from the descriptions of the SHGCs.

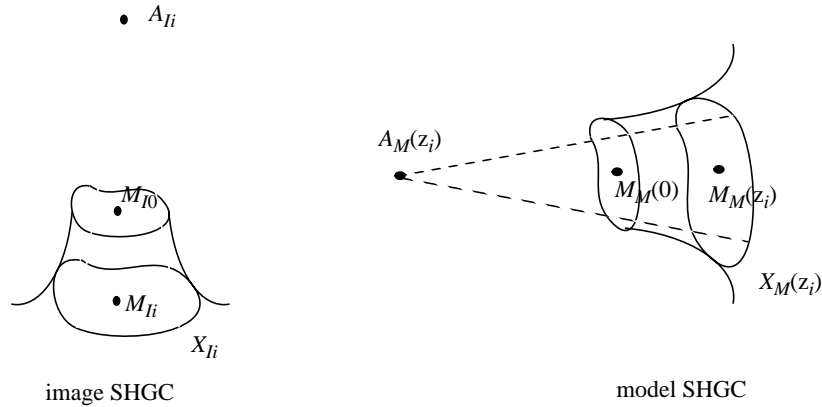


Figure 8.6 Finding axes points correspondences between image and model SHGCs

In the case where the SHGC axis passes through the cross-section mean (centered SHGC) then additional point correspondences can be determined. A correspondence can be established between the mean,  $M_{Ii}$ , of each cross-section  $X_{Ii}$  and the mean,  $M_M(z_i)$ , of the corresponding cross-section  $X_M(z_i)$ . This stems from the fact that, under scaled orthography, the projection of the mean of a closed planar curve is the mean of the projection of the curve. This results in the correspondences

$$\{(M_{Ii}, M_M(z_i)) \ i=0 \dots n\}$$

Figure 8.7 shows the correspondences ( $A_{Ii}$ ,  $A_M(z_i)$ ) and ( $M_{Ii}$ ,  $M_M(z_i)$ ) for the SHGC of the mug in the back of Figure 8.1 (whose origin coincides with the cross-section mean).

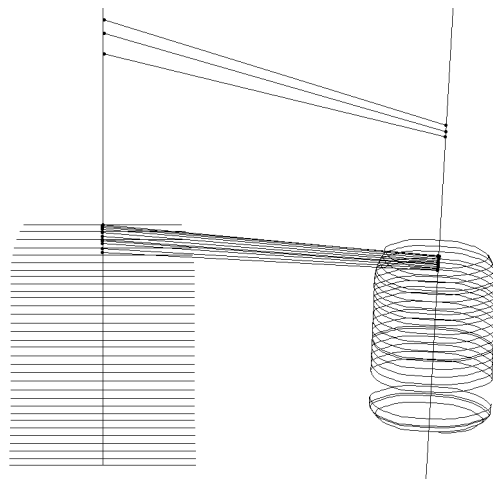


Figure 8.7 Image-model SHGC axis correspondences

### 8.3.2.1.2 Linear SHGCs

For a conical LSHGC, the local apexes are all a single point (the cone apex). Thus, the set of correspondences between image and model local apexes is a singleton  $\{(A_{I0}, A_M(0))\}$ . However, the set of correspondences between image and model cross-section means  $(M_{Ii}, M_M(z_i))$  includes all visible image cross-sections.

For a cylindrical LSHGC, the local apexes are all at infinity and thus cannot be used. The set of correspondences between image and model cross-section means has two elements, mapping the image and model means of the top and bottom cross-sections of the cylinder. We thus assume that a cylinder does not have a full portion of its surface occluded (it can still be partially occluded such that the full description can be inferred [145]).

### 8.3.2.2 PRGCs

The image description of an isolated PRGC is not as rich as the one of an isolated SHGC. The main reason is that, unlike with an SHGC, the scaling ratios cannot be determined in the image. In case enough “special” axis points, such as inflections or cross-section corners, exist (and can be identified) then correspondences can be established between image and model PRGCs. But this is not guaranteed. In general, though, it is observed that PRGCs are attached to other parts (serving for example, as handles, etc.). Thus, we choose to discuss PRGCs as part of composite objects.

## 8.3.3 Establishing Correspondences for Multi-Parts Objects

In some (but practically rare) situations, such as non-centered SHGCs, the sets of points  $M_{Ii}$  and  $A_{Ii}$  may not be colinear and thus they are sufficient to find the pose of a part (and the whole object if assumed rigid). However, in most cases, a multi-part object typically provides more information about the pose of all its parts, than each one of them does individually. For example, for the mug of Figure 8.1 (back), the presence of the handle conveys the pose of the symmetric cup, whose rotation about its axis is ambiguous when considered alone (the points used for the cup correspondences are all colinear; Figure 8.7).

In this case, we need at least one additional point correspondence which is not colinear with the SHGC axes. Below, we discuss the use of a PRGC attached to an SHGC. The case of two attached (non-colinear) SHGCs is similar. In case, more than two parts exist, any choice of non-colinear axes is equally valid.

Let us denote  $PRGC_I$  and  $PRGC_M$  the matched image and model PRGCs respectively. In case the axes of  $PRGC_I$  and  $PRGC_M$  have inflections, then they can simply be used as “distinguished” points to put into correspondence. In case the axes do not have inflections, then we assume that the object’s SHGC axis is contained in the PRGC axis plane, as is the case for many objects (due to physical stability reasons).

In the latter case, the tangent line at each point  $P_j$  ( $p_j$ ) of the axis of  $PRGC_M$  ( $PRGC_I$ ) is either parallel to the axis of  $SHGC_M$  ( $SHGC_I$ ) or intersects its supporting

line at some point  $B_{Mj}$  ( $B_{Ij}$ ). Thus, given an image point  $B_{Ij}$  (possibly at infinity), if we can determine the corresponding point  $B_{Mj}$  then we have a correspondence between  $p_j$  and  $P_j$  (see Figure 8.8). But, using the previously matched points on the SHGC axes, we can construct corresponding basis vectors  $V_I$  and  $V_M$  on the axes of SHGC<sub>I</sub> and SHGC<sub>M</sub>, respectively, with respect to which we can identify corresponding points by the same 1-D coordinate ( $\alpha$ ) along any of these vectors. Thus, given a point  $B_{Ij}$  and its coordinate  $\alpha_j$  (i.e.  $B_{Ij} = \alpha_j V_I$ ),  $B_{Mj}$  is given by

$$B_{Mj} = \alpha_j V_M. \quad (8.5)$$

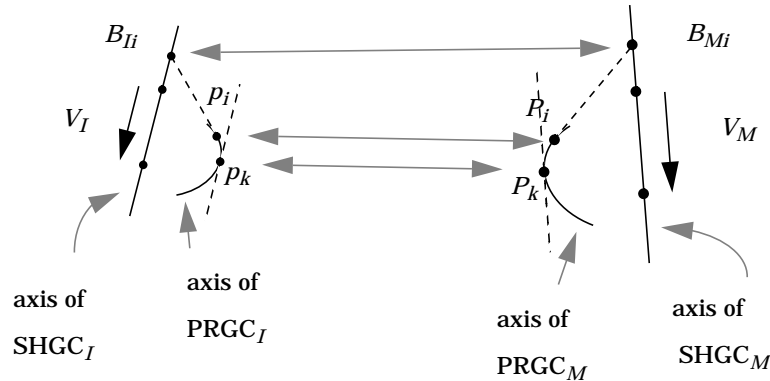


Figure 8.8 Using the SHGC axes correspondences to find PRGC axes correspondences.

In case  $\alpha_j \rightarrow \infty$  (i.e. the tangent at  $p_j$  is parallel to SHGC<sub>I</sub>'s axis), then the corresponding point  $P_j$  should also have its tangent parallel to SHGC<sub>M</sub>'s axis. Thus, through the coordinates of points on the SHGC axes, we can now establish an arbitrary number of point correspondences between the axes of PRGC<sub>I</sub> and PRGC<sub>M</sub> (points whose tangents pass through  $B_{Ij}$  and  $B_{Mj}$ ).

Figure 8.9 shows a correspondence, for the back object in Figure 8.1, between the axes points of PRGC<sub>I</sub> and PRGC<sub>M</sub> whose tangent lines are parallel to the SHGC axes.

### 8.3.4 Solving for the Pose Parameters

The image-model point correspondences obtained as described above are not all colinear. A choice of three non-colinear points should be sufficient to determine the 6 pose parameters as discussed by [134]. Here, we briefly review the method.

The angle  $\theta$  can be determined directly from the image and is given by the orientation of the image SHGC axis. Also, using only the image-model SHGC axes correspondences  $(u_j, v_j)^t, (0, 0, z_j)^t, j = 1, \dots, m$ , we can determine  $t_x, t_y$  using a least squares formulation which results in:

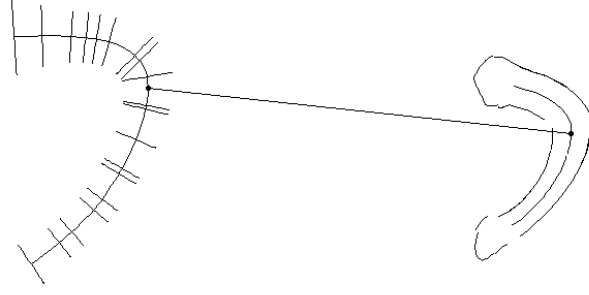


Figure 8.9 An example of image-model PRGC axes correspondence (the corresponding points have tangents parallel to the SHGC axes).

$$t_x = \frac{-\eta \sin \theta \sum_j z_j + \sum_j u_j}{m} ; t_y = \frac{\eta \cos \theta \sum_j z_j + \sum_j v_j}{m} \quad (8.6)$$

where

$$\frac{m \sum_j z_j (\sin \theta u_j - \cos \theta v_j) + \sum_j z_j (\cos \theta \sum_j v_j - \sin \theta \sum_j u_j)}{m \sum_j z_j^2 - (\sum_j z_j)^2} \quad (8.7)$$

Let  $p_a = (u_a, v_a)^t$  and  $P_a = (x_a, 0, z_a)^t$  be any pair of matched points not colinear with the above points (for example, the matched points on the image and model PRGC axes, respectively; without loss of generality, the coordinate system of  $PRGC_M$  is rotated such that its axis plane contains SHGC $_M$ 's  $i$ -axis).

Combining equations (8.3) (8.4), and (8.7), it can be shown that we obtain the quadratic form on  $\lambda$  (see [134] for the details of the mathematical formulation):

$$\eta^2 x_a^2 \lambda^2 - [\eta^2 x_a^2 + W_u^{a2} + (\eta z_a + W_v^a)^2] \lambda + W_u^{a2} = 0 \quad (8.8)$$

where  $u_a - t_x = W_u^a$ ,  $v_a - t_y = W_v^a$ , and  $\lambda = \cos^2 \phi$ .

For each solution  $\phi = \pm \cos^{-1} (\pm \sqrt{\lambda})$  (if a solution  $0 \leq \lambda \leq 1$  exists),  $\sigma$  and  $k$  can be determined by

$$\sigma = \tan^{-1} \left( \frac{\eta x_a \sin \phi}{\eta z_a + W_v^a} \right) + \delta \pi; k = \quad (8.9)$$

where  $\delta = 0$  or  $1$  depending on which results in a positive value of  $k$ .

Although the formulation of [134] leaves two possible solutions when three points are used, in our case we can uniquely determine the solution from the rich descriptions used. The solution is selected based on the image labeling of a part's cross-section as facing "towards" ( $\sigma > \frac{\pi}{2}$ ) or "away" ( $\sigma < \frac{\pi}{2}$ ) from the camera (this information is given from the types of junctions which terminate a part). This is another important use of the high-level descriptions in finding the 3-D pose.

The application of this method to the objects of Figure 8.1 is shown in Figure 8.10 showing the transformed and projected model objects (with cross-sections and meridians) on the image. Additional results are shown in Figure 8.11.

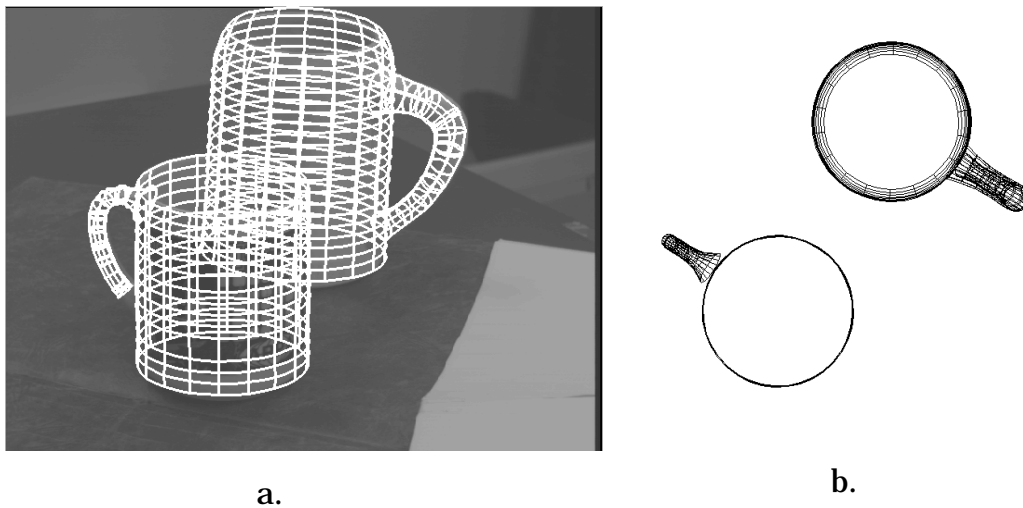


Figure 8.10 Overlay of the model objects with their estimated poses on the intensity image of Figure 8.1. (a); a top view of the objects (b).

## 8.4 Conclusion

The pose estimation method exploits the rich GC descriptions in order to establish (viewpoint invariant and quasi-invariant) point correspondences between axes, cross-sections and scaling functions of image and model parts. For the class of shapes addressed here, this results in a closed-form solution and avoids complex methods used in past work on curved objects.

In the near future, we plan to extend the method in several ways. Although the class of objects demonstrated in this paper is more complex than demonstrated in earlier work on curved objects, we plan to extend the method to more general classes, including non-exact primitives. Additionally, we plan to develop an indexing strategy in order to handle large databases. The indexing scheme should also be based on the part-based descriptions of the extracted objects.

Finally, we plan to integrate the current method into a larger framework of "recognition by hierarchical classes". In this framework, the similarity of the image objects is evaluated with respect to known generic classes starting from generic class

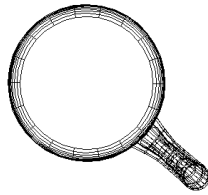
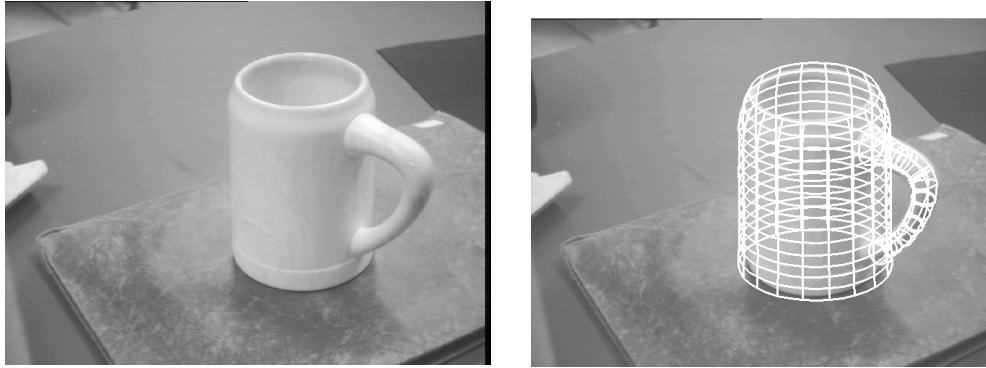


Figure 8.11 Another image of a previous object (back object of Figure 8.1) and its estimated pose.

descriptions and ending at specific object instances. Recognition and pose estimation would then proceed from qualitative criteria, using class descriptions, to quantitative ones, using object instances as shown in this paper. This is important for tasks such as learning and database organization. We expect the representations we use to allow us to make rapid progress on these issues.

## References

- [129]R. Bergevin and M.D. Levine. Generic Object Recognition: Building Matching and Coarse Descriptions from Line Drawings. *IEEE Transactions PAMI*, 15, pages 19-36, 1993.
- [130]R. A. Brooks. Model-Based Three Dimensional Interpretation of Two Dimensional Images. *IEEE Transactions on Pattern Analysis and Machine Intelligence*, 5(2):140-150, 1983.
- [131]M. Dhome, JT. Lapreste, G. Rives and M. Richetin, "Spatial localization of modelled objects revolution in monocular perspective vision," In Proceedings of *EC-CV*, pages 475-485, 1990.
- [132]S. Dickinson, 3-D shape Recovery using Distributed Aspect Matching, *IEEE Transactions PAMI*, 14(2):174-198, 1992.
- [133] *Geometric Invariance in Computer Vision*, J.L. Mundy and A. Zisserman editors, MIT Press, 1992.

- [134]D. P. Huttenlocher and S. Ullman, Recognizing Solid Objects by Alignment with an Image, *IJCV* 5, 195-212, 1991.
- [135]W.E.L. Grimson, *Object Recognition by Computer-The Role of Geometric Constraints*, MIT Press, Cambridge MA 1990.
- [136]D.J. Kriegman and J. Ponce, "On recognizing and positioning curved 3-D objects from image contours," in *IEEE Transactions of PAMI*, pages 1127-1137, (12) 1990.
- [137]J. Liu, J. Mundy, D. Forsyth, A. Zisserman and C. Rothwell, Efficient Recognition of Rotationally Symmetric Surfaces and Straight Homogeneous Generalized Cylinders, In *Proceedings of IEEE Computer Vision and Pattern Recognition*, pages 123-128, 1993.
- [138]D. G. Lowe, "The viewpoint consistency constraint, " *IJCV*, pages 57-72, 1987.
- [139]J.L. Mundy, C. Huang, J. Liu, W. Hoffman, D.A. Forsyth, C.A. Rothwell, A. Zisserman, S. Utcke, and O. Bournez, MORSE: A 3-D object recognition system based on geometric invariants, *IJCV*, 1393-1402. 1994/
- [140]R. Nevatia and T.O. Binford, Description and Recognition of Complex Curved Objects, *Artificial Intelligence*, 8(1):77-98, 1977.
- [141]A. Pentland. Recognition by Parts. in *Proceedings of the ICCV*, pages 612-620, 1987.
- [142]L. Roberts. *Machine Perception of Three-Dimensional Solids*. MIT Press, 1965.
- [143]F. Ulupinar and R. Nevatia, Perception of 3-D Surfaces from 2-D Contours, *IEEE Transactions PAMI*, pages 3-18, 15, 1993.
- [144]M. Zerroug and R. Nevatia, "Quasi-invariant Properties and 3-D Shape Recovery of Non-Straight, Non-Constant Generalized Cylinders", In *Proceedings of CVPR*, pages 96-103. 1993. New York.
- [145]M. Zerroug and R. Nevatia, "Segmentation and 3-D Recovery of SHGCs from a Single Intensity Image, in *Proceedings of the ECCV*, pages 319-330, Stockholm, 1994.
- [146]M. Zerroug and R. Nevatia, "From an Intensity Image to 3-D Segmented Descriptions" In *Proceedings of the ICPR*, 1994.